International Journal of Non-Linear Mechanics ▮ (▮▮▮▮) ▮▮▮–▮▮▮

Contents lists available at ScienceDirect

International Journal of Non-Linear Mechanics

journal homepage: www.elsevier.com/locate/nlm

# Elastocapillary imbibition

Jeffrey M. Aristoff *, Camille Duprat, Howard A. Stone

*Department of Mechanical and Aerospace Engineering, Princeton University, Princeton, NJ 08544, USA*

ARTICLE INFO

*Keywords:*
Elastocapillarity
Wicking
Coalescence
Surface tension
Free-boundary problem

ABSTRACT

When a wetting liquid invades a porous medium or a capillary tube, the penetration or imbibition speed is known to decrease as the square root of time. We examine the capillary filling of a gap between flexible sheets and demonstrate that the pressure-induced inward deflection of the sheets leads to a non-monotonic behavior of the speed of the invading meniscus until eventually the flow is blocked. A model based on lubrication theory is formulated as a non-linear free-boundary problem, which is solved numerically using finite-difference methods. Good agreement is obtained with our experiments. At early times the deformation of the sheets is insignificant, and the penetration speed is unaffected. At later times, as the penetration distance approaches the elastocapillary length, the deformation becomes appreciable and the flow accelerates. Shortly thereafter, the gap at the air–liquid interface goes to zero, and the flow necessarily stops. The length of the sheets above which imbibition will cause them to coalesce is determined and is found to be in good agreement with that predicted via scaling arguments. Biological applications of this transient wetting of flexible boundaries are discussed.



## 1. Introduction

The surface-tension-driven coalescence of flexible structures, i.e., elastocapillarity, is relevant to a number of biological and engineering processes, such as the closure of pulmonary airways [1–3], the design of biomimetic adhesives [4,5], the failure of micro and nanoscale devices [6–9], and the stability of water-walking arthropods [10]. Elastocapillarity has been the subject of several recent studies that analyze equilibrium configurations where there is a balance between elasticity and capillarity. Bico et al. [11] and Kim and Mahadevan [12], for example, investigated the statics of capillary rise of a liquid between flexible sheets, and Kwon et al. [13] examined the shape of a liquid drop confined beneath a flexible sheet. To the best of our knowledge, the transient wetting of flexible boundaries has been considered by relatively few authors. Siddique et al. [14] investigated the dynamics of capillary rise into a deformable porous material, while van Honschoten et al. [15] studied the capillary filling, or *imbibition*, of a nanochannel with an elastic capping layer. In this paper we consider imbibition between flexible sheets, and we determine a criterion for their coalescence. In particular, we quantify the time-dependent deflection of the sheets and the penetration speed of the invading liquid as it advances towards the initially free end of the sheets.

Consider the capillary filling of a gap between flexible, inextensible sheets of thickness $b$, width $w$ (into the page) and length $\ell$ that are initially parallel and separated by a distance $2h_0$, as depicted in Fig. 1. The sheets are clamped at their left end, where fluid enters from a reservoir at atmospheric pressure, so that the flow into the gap between the sheets is driven solely by surface tension owing to a reduction in pressure at the meniscus; gravitational effects are neglected. The pressure distribution associated with the invasion of fluid leads to an inward deflection of the sheets, which further alters the pressure distribution in the liquid and the speed at which the meniscus advances. The shape of the sheet is denoted $h(z,t)$, and the penetration distance or meniscus position $z_m(t)$.

The characteristic length scale over which the sheets will deflect to a combined distance of $2h_0$ may be estimated by taking each sheet to be a cantilever that is loaded at a distance $\ell_{ec}$ from its clamped end by the Laplace pressure $\gamma\kappa$, where $\gamma$ is the surface tension. The curvature at the meniscus may be approximated by $\kappa = \cos\theta_e/h(z_m) + \cos\theta_e/(w/2)$, where $\theta_e$ is the contact angle (imbibition requires $\theta_e < \pi/2$) [16]. By taking $h(z_m,t) = h_0$, $h_0 \ll w$, and by using the Euler–Bernoulli beam equation $Bh_{zzzz} = \gamma\kappa$, where subscripts denote derivatives, $B = Eb^3/12(1-\nu^2)$ is the bending stiffness per unit width, $E$ the Young's modulus, and $\nu$ the Poisson ratio, we identify the characteristic length scale

$$\ell_{ec} = \left(\frac{Bh_0^2}{\gamma\cos\theta_e}\right)^{1/4}, \tag{1}$$

which may be interpreted as an elastocapillary length. This particular length scale is also relevant to the coalescence of wet hair [11], and the adhesion-related failure of micromechanical

* Corresponding author.
*E-mail address:* aristoff@princeton.edu (J.M. Aristoff).

0020-7462/$ - see front matter © 2010 Elsevier Ltd. All rights reserved.
doi:10.1016/j.ijnonlinmec.2010.09.001

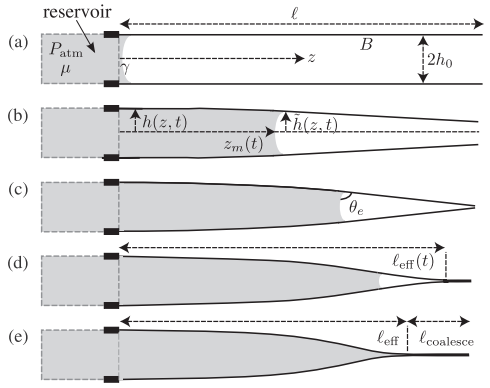


**Fig. 1.** Sketch of elastocapillary imbibition. (a) Liquid (shaded region) with viscosity $\mu$ and surface tension $\gamma$ enters the region between two clamped sheets with length $\ell$ and bending stiffness per unit width $B$, which are separated by a distance $2h_0$. (b) The liquid wets the sheets, which subsequently deflect inward owing to a reduction in pressure and the force $2w\gamma\sin\theta_e$ at the contact line. The shape of the wetted region of the sheet is denoted by $h(z,t)$, the dry region of the sheet by $\tilde{h}(z,t)$, and the position of the invading meniscus by $z_m(t)$. (c) The ends of the sheet touch and exert a force on each other. (d) The sheets coalesce over the length $\ell-\ell_{\rm eff}(t)$. (e) Imbibition continues until the liquid entirely fills the region between the sheets, resulting in coalescence over the length $\ell_{\rm coalesce}$.

devices during drying [17]. Specifically, $\ell_{ec}$ is the length of the object above which capillary-driven coalescence occurs.

The characteristic time scale may be estimated by using Darcy's law,

$$\frac{\mu u}{k} = -\frac{\partial p}{\partial z}, \tag{2}$$

where $\mu$ is the kinematic viscosity, $u$ the cross-sectionally averaged liquid velocity, $k=h^2/3$ the permeability, $p$ the local pressure, and $z$ the axial coordinate. Combining (2) with one-dimensional mass conservation,

$$h_t + (hu)_z = 0, \tag{3}$$

and relating the deflection to the Laplace pressure at the meniscus gives the characteristic time scale

$$t_c = \left(\frac{9B\mu^2}{\gamma^3\cos^3\theta_e}\right)^{1/2}. \tag{4}$$

For early times $t \ll t_c$, or equivalently where the position of the meniscus $z_m(t) \ll \ell_{ec}$, we expect the deflection of the sheets to be negligible and the meniscus to advance according to that given by the classical (capillary) imbibition result [18]:

$$z_m(t) = \left(\frac{2\gamma\cos\theta_e h_0}{3\mu}\right)^{1/2} t^{1/2} \tag{5}$$

and

$$\frac{dz_m}{dt} = \left(\frac{\gamma\cos\theta_e h_0}{6\mu}\right)^{1/2} t^{-1/2}. \tag{6}$$

For later times $t < t_c$, or equivalently $z_m < \ell_{ec}$, we expect the sheet to deflect considerably and the meniscus speed to deviate from that predicted by (6). Finally, as $t$ approaches $t_c$, or equivalently $z_m \approx \ell_{ec}$, we expect the gap at the meniscus to reach zero, and the flow to therefore stop.

## 2. Theoretical formulation

We proceed by deriving an evolution equation for the sheet deformation, $h(z,t)$, and fluid velocity, $u(z,t)$, by treating the flow as incompressible and one-dimensional in the axial or $z$-direction. The viscously dominated dynamics are described by Darcy's law, given by (2), where we have estimated the permeability $k$ based on the lubrication approximation [19] which requires $|h_z| \ll 1$. Since this approximation implies that the slope of the sheets is small, we may use the linear theory of plates to describe their deformation. Due to symmetry about the $z$-axis, we need to consider only one of the sheets. Provided further that the sheet is sufficiently thin, $b \ll w \ll \ell$, its deflection is described by the Euler–Bernoulli beam equation,

$$Bh_{zzzz} = q(z,t), \tag{7}$$

where we have neglected the inertia of the sheet and its weight, and $q(z,t)$ is the force per unit area (pressure) acting on the sheet [20]. This quasi-static description of the sheet is appropriate provided that the characteristic time scale of the flow, $t_c$, is much longer than the reaction time of the sheet to an applied load, $\tau = \sqrt{\rho_s b\ell^4/B}$. The reaction time is found by equating the bending energy $B(h_0/\ell^2)^2\ell w$ to the inertial stress $\rho_s bw\ell(h_0/\tau)^2$, where $\rho_s$ is the density of the sheet. The weight of the beam may be neglected provided that the gravitational torque $\rho_s bw\ell^2 g\cos\alpha$ is much less than the bending moment $Bwh_0/\ell^2$, or equivalently $\rho_s b\ell^4 g\cos\alpha/Bh_0 \ll 1$, where $\alpha$ is the initial inclination of the sheet with respect to the horizontal.

### 2.1. Deflection of the liquid-filled region $h(z,t)$

We first consider the deflection of the sheet where it is in contact with the liquid. The flow is from left to right. To the left of the meniscus, $0 \le z \le z_m(t)$, we may differentiate (7) and combine it with (2) to obtain

$$u(z,t) = -\frac{B}{3\mu}h^2 h_{zzzzz}. \tag{8}$$

We evaluate (8) at $z=z_m$ to find an expression for the motion of the meniscus:

$$\frac{dz_m}{dt} = -\frac{B}{3\mu}h^2 h_{zzzzz}\Big|_{z=z_m}. \tag{9}$$

Next, combining (8) with the statement of mass conservation, given by (3), yields the non-linear evolution equation

$$h_t = \frac{B}{3\mu}(h^3 h_{zzzzz})_z. \tag{10}$$

Eq. (10) was studied by Hosoi and Mahadevan [21], who considered the dynamics of an elastic sheet that was clamped at one end and lubricated from below by a single fluid. Our study is distinguished by the presence of two fluids (air and liquid) in the lubricating layer, and the additional equation for the time-dependent position of the air–liquid interface, given by (9). Before we discuss the boundary conditions for (10), we consider the deflection of the liquid-free region.

### 2.2. Deflection of the liquid-free region $\tilde{h}(z,t)$

To the right of the meniscus, $z_m(t) < z \le \ell$, the deflection of the sheet $\tilde{h}(z,t)$ is given by

$$B\tilde{h}_{zzzz} = 0, \tag{11}$$

which may be integrated analytically to give

$$\tilde{h}(z,t) = c_1(t)(z-z_m)^3 + c_2(t)(z-z_m)^2 + c_3(t)(z-z_m) + c_4(t). \tag{12}$$

The unknown coefficients $c_1$, $c_2$, $c_3$, and $c_4$ will be determined by the boundary conditions at the free end $z=\ell$ and the matching conditions with the wetted portion of the sheet at $z=z_m$.

Please cite this article as: J.M. Aristoff, et al., Elastocapillary imbibition, Int. J. Non-Linear Mech. (2010), doi:10.1016/j.ijnonlinmec.2010.09.001

### 2.3. Boundary conditions

The boundary conditions for (10) and (12) will now be specified. The left end of the sheet is assumed to be fixed and clamped, and the pressure is atmospheric. Correspondingly,

$$h(0,t)=h_0, \quad h_z(0,t)=0, \quad \text{and} \quad h_{zzzz}(0,t)=0. \tag{13}$$

At the meniscus, $z=z_m$, there is a jump in pressure equal to the Laplace pressure, which may be written in the form

$$Bh_{zzzz}(z_m,t)-B\tilde{h}_{zzzz}(z_m,t)=-\frac{\gamma\cos\theta_e}{h(z_m,t)}. \tag{14}$$

Initially, the right-most end of the sheet is force- and moment-free. Thus, both the shear and curvature at the right-most end are zero,

$$\tilde{h}_{zz}(\ell,t)=0 \quad \text{and} \quad \tilde{h}_{zzz}(\ell,t)=0, \tag{15}$$

so we must have $c_1=0$ and $c_2=0$ in (12). At the meniscus, the position and slope are continuous, requiring that $c_4=h(z_m,t)$ and $c_3=h_z(z_m,t)$. The curvature must also be continuous, so that

$$h_{zz}(z_m,t)=\tilde{h}_{zz}(z_m,t)=0. \tag{16}$$

Due to surface tension acting along the contact line, there is a jump in the transverse shear force at the meniscus, so that

$$Bh_{zzz}(z_m,t)-B\tilde{h}_{zzz}(z_m,t)=-\gamma\sin\theta_e. \tag{17}$$

We note that for a purely wetting liquid, $\theta_e=0$, and (17) reduces to $h_{zzz}(z_m,t)=0$.

The tips of the sheet will contact at a time $\hat{t}$ when $\tilde{h}(\ell,t)=0$. Should this occur, the sheets exert an equal but opposite force on each other, and the shear-free boundary condition at $z=\ell$, (15b), must be replaced by the condition $\tilde{h}(\ell,t)=0$. The matching conditions at $z=z_m$ then require for $t\geq\hat{t}$ that (16) and (17) be replaced by

$$h_{zz}(z_m,t)=\frac{-3h_z(z_m,t)(\ell-z_m)-3h(z_m,t)}{(\ell-z_m)^2} \tag{18}$$

and

$$h_{zzz}(z_m,t)=\frac{3h_z(z_m,t)(\ell-z_m)+3h(z_m,t)}{(\ell-z_m)^3}-\frac{\gamma\sin\theta_e}{B}, \tag{19}$$

respectively. Finally, should the sheets touch over a segment $\ell_{\text{eff}}\leq z<\ell$, we must have $\tilde{h}(\ell_{\text{eff}})=\tilde{h}_z(\ell_{\text{eff}})=0$, consistent with a tangentially smooth contact. This condition, together with $\tilde{h}_{zz}(\ell_{\text{eff}})=0$, prescribes the value of $\ell_{\text{eff}}$ and requires that we replace $\ell$ by $\ell_{\text{eff}}$ in (18) and (19).

### 2.4. Non-dimensionalization

We proceed by non-dimensionalizing the evolution equations and boundary conditions using the characteristic length and time scales determined in Section 1. Let $H=h/h_0$, $Z=z/\ell_{ec}$, $Z_m=z_m/\ell_{ec}$, $L=\ell/\ell_{ec}$, and $T=t/t_c$. These substitutions transform the evolution equations, given by (9) and (10), to

$$\frac{dZ_m}{dT}=-H^2H_{ZZZZZ}\Big|_{Z=Z_m} \tag{20}$$

and

$$H_T=(H^3H_{ZZZZZ})_Z, \tag{21}$$

respectively. The boundary conditions, given by (13a), (13b), (13c), (14), (16) and (17), become

$$H(0,T)=1, \tag{22a}$$

$$H_Z(0,T)=0, \tag{22b}$$

$$H_{ZZZ}(0,T)=0, \tag{22c}$$

$$H_{ZZZ}(Z_m,T)=-\frac{1}{H(Z_m,T)}, \tag{22d}$$

$$H_{ZZ}(Z_m,T)=0 \quad \text{and} \tag{22e}$$

$$H_{ZZZ}(Z_m,T)=-\Upsilon, \tag{22f}$$

where

$$\Upsilon=\left(\frac{h_0}{\ell_{ec}}\right)\tan\theta_e. \tag{23}$$

For the case when the sheets contact, the boundary conditions (18) and (19) become

$$H_{ZZ}(Z_m,T)=\frac{-3H_Z(Z_m,T)(L-Z_m)-3H(Z_m,T)}{(L-Z_m)^2} \tag{24}$$

and

$$H_{ZZZ}(Z_m,T)=\frac{3H_Z(Z_m,T)(L-Z_m)+3H(Z_m,T)}{(L-Z_m)^3}-\Upsilon, \tag{25}$$

respectively.

Since we have used (12) to express the matching conditions at the meniscus $Z=Z_m$ in terms of the boundary conditions at the end of the sheet $Z=L$, the solution of (20)–(25) for the liquid-filled region automatically satisfies the boundary conditions at $Z=L$, and prescribes the deflection of the liquid-free region, $Z_m<Z\leq L$,

$$\tilde{H}(Z,T)=H_Z(Z_m,T)(Z-Z_m)+H(Z_m,T), \tag{26}$$

where $\tilde{H}=\tilde{h}/h_0$. For the case that the sheets contact, the deflection of the liquid-free region is no longer given by (26), but instead by

$$\tilde{H}(z,T)=\frac{H_{ZZZ}(Z_m,T)+\Upsilon}{6}(Z-Z_m)^3+\frac{H_{ZZ}(Z_m,T)}{2}(Z-Z_m)^2 +H_Z(Z_m,T)(Z-Z_m)+H(Z_m,T) \tag{27}$$

for $Z\leq L_{\text{eff}}=\ell_{\text{eff}}/\ell_{ec}$, and $\tilde{H}(Z,T)=0$ otherwise.

For a perfectly wetting liquid we have $\Upsilon=0$. For a partially wetting liquid, provided that the gap is much smaller than the elastocapillary length, we may also take $\Upsilon=0$. Thus, we may safely neglect the influence of the contact angle on the dynamics, and so, in what follows, we take the dimensionless jump in the transverse shear force at the meniscus, $H_{ZZZ}(Z_m,T)=0$. Thus, by choosing the proper length and time scales to non-dimensionalize the governing equations and boundary conditions, we have eliminated all physical parameters from (20)–(22). Although the parameter $L$ appears in the boundary conditions (24) and (25), we shall observe below that its value has little influence on the overall dynamics of elastocapillary imbibition, provided that $L\gtrsim 2.9$. Therefore, in a practical sense the dimensionless solution reported here is universal.

## 3. Numerical solution

### 3.1. Numerical method

The evolution equations (20) and (21), together with the boundary conditions (22)–(25), are solved numerically for $H(Z,T)$ and $Z_m(T)$ using a finite-difference method implemented in MATLAB®. In order to do so, we first map the time-dependent interval $0\leq Z\leq Z_m(T)$ to the fixed interval $0\leq S\leq 1$ by making the substitution $S=Z/Z_m(T)$. We then choose an implicit scheme (backwards in time, centered in space) to discretize the resulting evolution equations and boundary conditions. This choice provides accuracy of $O(\Delta S^2)$ in space and $O(\Delta T)$ in time, where $\Delta S$ is

Please cite this article as: J.M. Aristoff, et al., Elastocapillary imbibition, Int. J. Non-Linear Mech. (2010), doi:10.1016/j.ijnonlinmec.2010.09.001

the increment in space, and $\Delta T$ is the increment in time. Forward and backward finite-difference approximations of order $O(\Delta S^2)$ are used to incorporate the boundary conditions at $S=0$ and 1, respectively. For each term in (20)–(25) that is non-linear, the lowest order derivatives are found using the corresponding explicit finite-difference approximation. Numerical tests were performed to verify stability and convergence of the chosen scheme. The initial conditions $H(S,0.00125)=1$ and $Z_m(0.00125)=0.05$ were used throughout the study, consistent with the classical prediction $Z_m=\sqrt{2}T^{1/2}$ that is valid for $Z_m \ll 1$. As in classical imbibition, we cannot take $Z_m(0)=0$, which would lead to an ill-posed problem as a finite force is applied to an infinitesimal mass. For a typical $\Delta T=10^{-3}$ and $\Delta S=\frac{1}{30}$, the numerical solution is obtained within 1 min on a 2 GHz processor.

### 3.2. Numerical results

We present the time-evolution of the deflection of the sheets in Fig. 2 for three sheets having different lengths $L$. The liquid-filled region has been shaded. Initially, the gap thickness is uniform, i.e., the sheets are parallel. As time increases, the meniscus advances and the sheets deflect inward. The shortest sheets ($L=1.5$) do not coalesce during imbibition (Fig. 2a), and the flow stops once the meniscus reaches the end of the sheets. The longer sheets ($L=2.2$) coalesce during imbibition (Fig. 2b), but the distance over which they coalesce is small relative to the length of the sheet. The longest sheets ($L=5$) coalesce over a large distance during imbibition (Fig. 2c).

A comparison between elastocapillary imbibition and capillary-driven (classical) imbibition is presented in Fig. 3 for $L=\ell/\ell_{ec}=1.5$ (solid gray curves), $L=2.2$ (dashed gray curves), and $L=5$ (dash-dotted gray curves). At early times, $T \ll 1$, the penetration distance, shown in Fig. 3a, follows the classical prediction, given by (5). At later times, when $T = O(1)$, the penetration distance increases relative to the classical prediction, denoted by the black line, and the penetration speed necessarily increases. This relative increase is observed in Fig. 3b, where we present the penetration speed versus time. An acceleration of the imbibing front is observed for each of the three cases. The gap at the meniscus as a function of time is shown in Fig. 3c. We note that for $L=1.5$, imbibition stops when the meniscus reaches the end of the sheets, an event that occurs prior to the gap at the meniscus reaching zero. For $L=2.2$ and $L=5$, we find that the penetration speed goes to zero in finite time, contrary to the classical prediction, given by (6), where the elastocapillary length

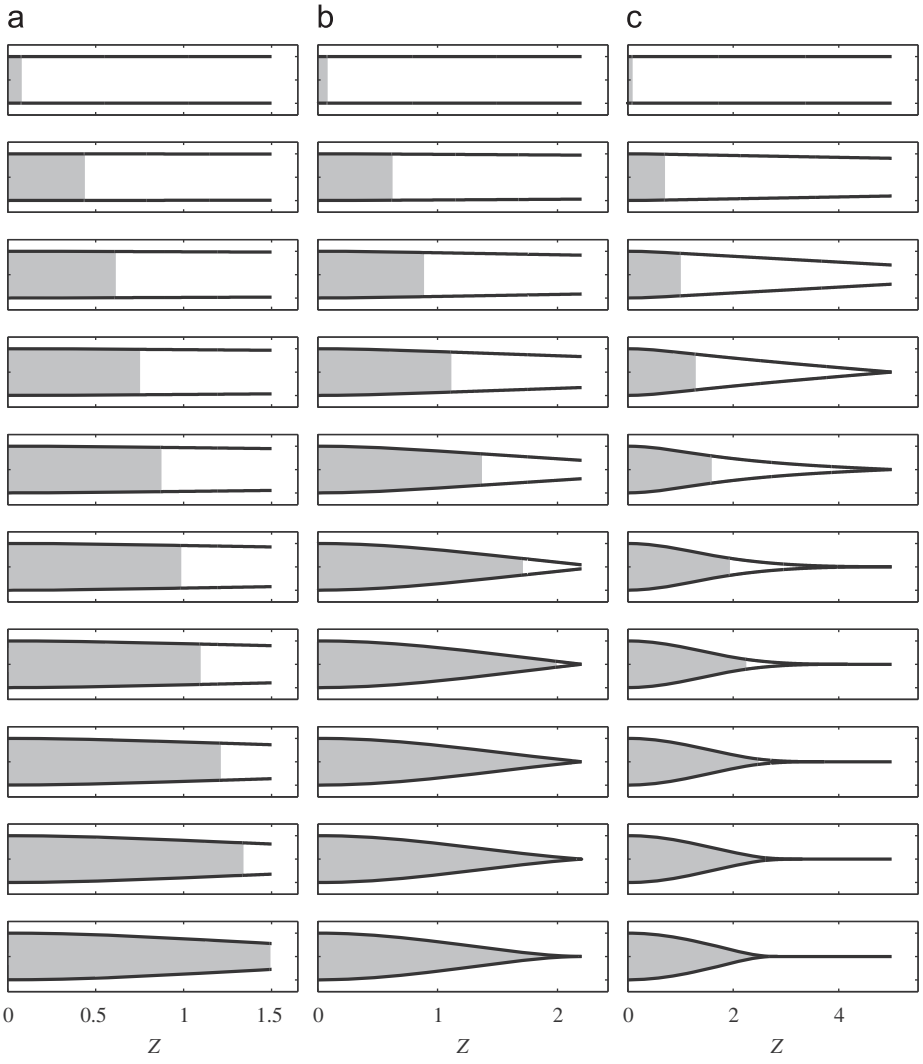


**Fig. 2.** Time-series plot of the upper and lower sheet profiles, $H(Z,T)$ and $-H(Z,T)$, as the sheet length is increased through $L=\ell/\ell_{ec}=1.5$, $L=2.2$, and $L=5$. The meniscus advances from left to right. The final frame corresponds to the time at which the meniscus stops. (a) The time between successive images is $T=t/t_c=0.09$. (b) The time between successive images is $T=0.184$. (c) The time between successive images is $T=0.228$.

Please cite this article as: J.M. Aristoff, et al., Elastocapillary imbibition, Int. J. Non-Linear Mech. (2010), doi:10.1016/j.ijnonlinmec.2010.09.001

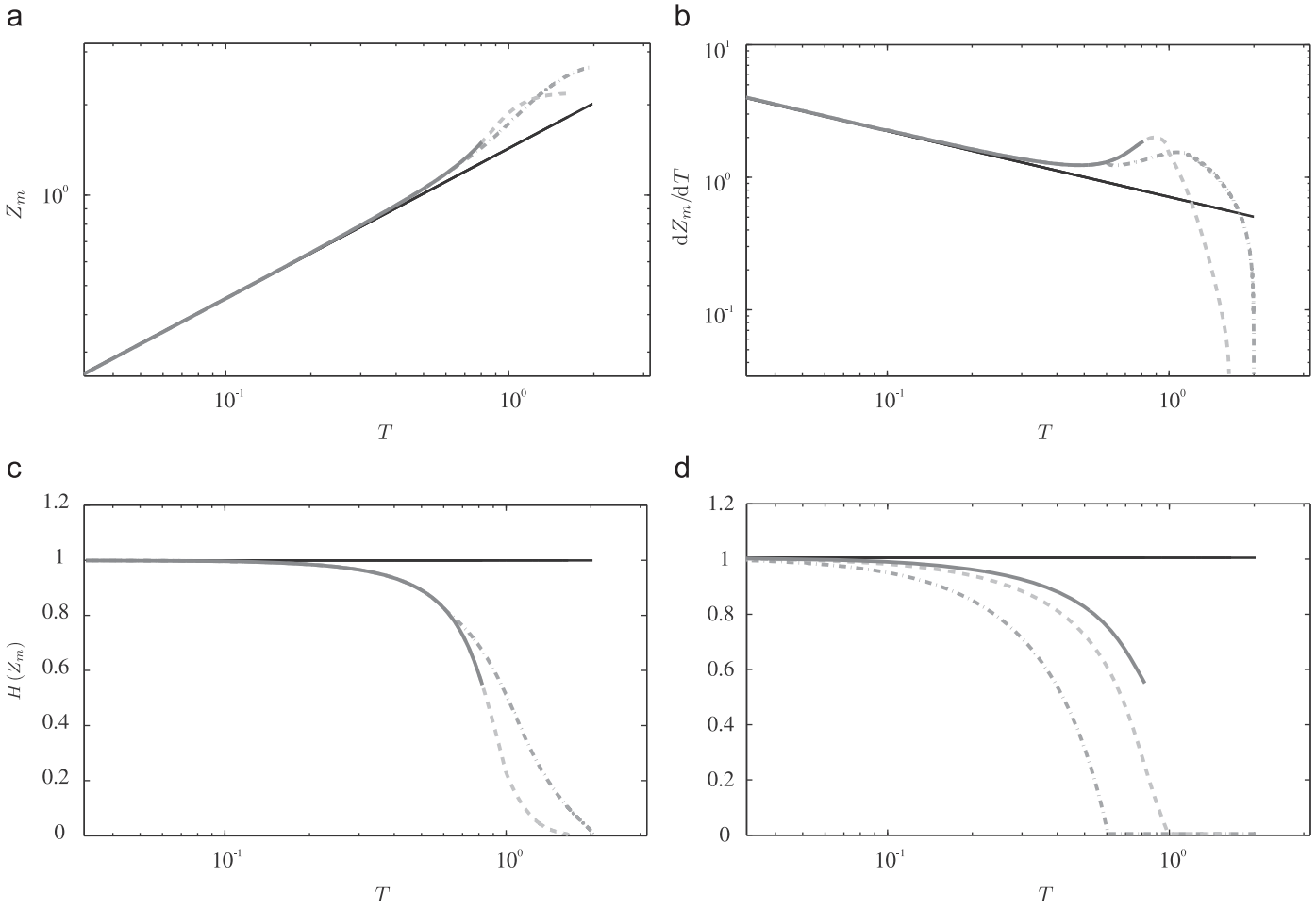


**Fig. 3.** Summary of numerical results for $L=\ell/\ell_{ec}=1.5$ (solid gray curves), $L=2.2$ (dashed gray curves), and $L=5$ (dash-dotted gray curves). (a) Penetration distance versus time. (b) Penetration speed versus time. (c) Gap at the meniscus versus time. (d) Gap at the initially free end of the sheet versus time. The black lines denote the classical prediction for the penetration distance, penetration speed, gap at $Z_m$, and gap at $L$, and are given by $Z_m=\sqrt{2}T^{1/2}$, $dZ_m/dT=(2T)^{-1/2}$, $H(Z_m)=1$, and $H(L)=1$, respectively. Deviations from these predictions occur when $T=O(1)$, or equivalently, when $Z_m=O(1)$.

is effectively infinite. Finally, in Fig. 3d we present the time evolution of the gap at $H=L$. For $L=1.5$ (solid gray curve), the sheets do not coalesce during imbibition, whereas for $L=2.2$ and $L=5$ (dashed and dash-dotted gray curves), imbibition causes the sheets to coalesce.

We further quantify the influence of the sheet length $L$ on elastocapillary imbibition in Fig. 4. The maximum penetration distance $Z_m^*$, the distance at which the flow stops, is denoted by the □ symbol. For short sheets, $L\leq 1.95$, we find $Z_m^*=L$, i.e., the front reaches the end with a finite separation distance between the sheets. For long sheets, $L>2.9$, we find that $Z_m^*$ reaches a constant value of 2.67 that is independent of $L$. The time at which imbibition stops, $T^*$, is denoted by the ◯ symbol, and also reaches a constant value (2.03) for sufficiently long sheets. Both $T^*$ and $Z_m^*$ achieve maximum values near $L=2.9$, at the boundary between regimes II and III, where the slope of the sheet reaches a minimum value (not shown). Coalescence occurs above a critical sheet length of $L\approx 1.95$, which is a value that is in good agreement with the $O(1)$ value predicted via scaling arguments.

The apparent independence of $Z_m^*$ and $T^*$ on the sheet length for $L\gg 1$ may be understood by examining the boundary conditions (24) and (25) in which $L$ enters the problem formulation. For $L\gg Z_m$, (24) reduces to $H_{ZZ}(Z_m,T)=0$ and (25) reduces to $H_{ZZZ}(Z_m,T)=0$. Thus, although the sheets make contact at $Z=L$, the shear force and curvature there are negligible, the boundary conditions become independent of $L$, and we may take (22e) and (22f) in favor of (24) and (25). Finally, we performed numerical tests to determine the range of validity of the lubrication approximation $|h_z|\ll 1$, or equivalently $|H_Z|(h_0/\ell_{ec})\ll 1$. In regime I we require $h_0/\ell_{ec}\ll 1$. In regime II we require $h_0/\ell_{ec}\ll 10^{-2}$. In regime III we require $h_0/\ell_{ec}\ll 10^{-1}$. Therefore, provided that ratio between the initial gap and the elastocapillary length is sufficiently small, the lubrication approximation is valid.

## 4. Experimental study

We have observed experimentally a deviation from classical imbibition by considering the capillary filling of a gap between flexible sheets. We discuss these results in the framework of the theoretical model presented in Section 2.

### 4.1. Experimental setup

A sketch of our experimental setup is shown in Fig. 5. Two horizontal glass sheets (thickness $b=160\,\mu$m, width $w=12$ mm and bending stiffness per unit width $B=2.2\times 10^{-2}$ N m) are clamped over a fixed length $\ell_0$ at one end, and free at the other. The sheets are initially parallel and separated by a distance $2h_0=0.37$ mm. The clamped end of the sheet is brought into contact with a bath of silicone oil (viscosities $\mu=0.048$ and 0.096 Pa s, surface tension $\gamma=0.021$ N m$^{-1}$) that perfectly wets the

Please cite this article as: J.M. Aristoff, et al., Elastocapillary imbibition, Int. J. Non-Linear Mech. (2010), doi:10.1016/j.ijnonlinmec.2010.09.001

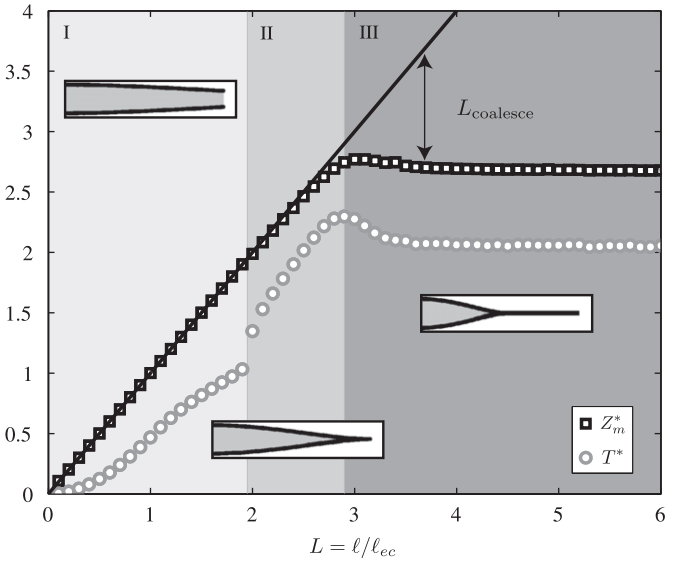


**Fig. 4.** Influence of the sheet length $L=\ell/\ell_{ec}$ on the imbibition dynamics and distance over which the sheets coalescence, $L_{\text{coalesce}}=\ell_{\text{coalesce}}/\ell_{ec}=L-Z_m^*$. The maximum penetration distance, $Z_m^*$, is denoted by the □ symbol. The time at which imbibition stops, $T^*$, is denoted by the ○ symbol. In regime I ($L\lesssim 1.95$), imbibition stops when the meniscus reaches the end of the sheet ($Z_m^*=L$). In regime II ($1.95<L\lesssim 2.9$), the sheets touch during imbibition, but the distance over which they contact, $L_{\text{coalesce}}$, is small relative to the length of the sheet. In regime III $=(L>2.9)$, both $Z_m^*$ and $T^*$ become nearly independent of $L$, and $L_{\text{coalesce}}$ thus increases linearly with $L$.

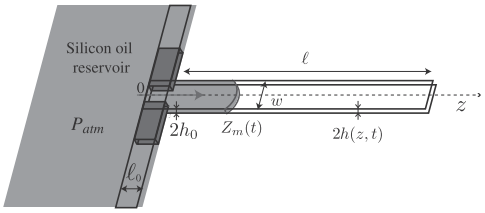


**Fig. 5.** Sketch of the experimental setup. The illustrated shape of the meniscus corresponds to a typical experimental observation.

glass ($\theta_e=0$). The material properties, the surface tension, and the initial gap are held constant, so that a constant elastocapillary length $\ell_{ec}=14.8$ mm is obtained. The ratio $L=\ell/\ell_{ec}$ is varied by changing the length of the sheets $\ell+\ell_0$.

The liquid is gently poured into the reservoir to start imbibition. The initial position of the meniscus $z_0=0$ and time $t_0=0$ correspond to the beginning of impregnation at the clamped edge of the sheets. The liquid advances in the rigid section of the channel and enters the region of interest (where the sheets are free to deflect) at a distance $z=\ell_0$. The position of the meniscus is recorded from above with a digital camera and tracked using a customized image-analysis program written in MATLAB®. The shape of the sheets is recorded from the side.

### 4.2. Results

Depending on the length of the sheets, four different behaviors are observed. For short sheets ($L\lesssim 0.6$), no bending is observed and classical imbibition is recovered. Nevertheless, the meniscus appears to advance slower than predicted by (5). Specifically, we find the relationship $z_m(t)=\alpha(2\gamma\cos\theta_e h_0/3\mu)^{1/2}t^{1/2}$, where $\alpha=0.58$. This discrepancy likely arises from the neglect of the contact-line dynamics in the derivation of (5), which would tend to flatten the meniscus at early times, and thus reduce the speed of imbibition [22]. A second contribution to the reduction in speed could result from the open sides of the channel or the finite width of the sheets. The correction prefactor $\alpha=0.58$ is roughly constant for all of our experiments.

For longer sheets, we observe a deviation from classical imbibition—the liquid appears to accelerate as the sheets come together. Image sequences of the deflecting sheets are provided in Fig. 6. We quantify this deviation in Fig. 7, where we plot the position and speed of the meniscus versus time.

In regime I ($0.6\lesssim L\lesssim 1.47$), the sheets do not touch during imbibition (Fig. 6a). At early times, the sheets remain parallel. The liquid invades the space between the sheets following a classical diffusive law (Fig. 7a). As the meniscus advances, we observe a deflection of the sheets, which subsequently leads to an acceleration of the meniscus. The flow stops when the meniscus reaches the end of the sheets, which remain open indefinitely.

The early time dynamics of regime II ($1.47\lesssim L\lesssim 2.5$) are similar to that of regime I. Nevertheless, the deflection of the

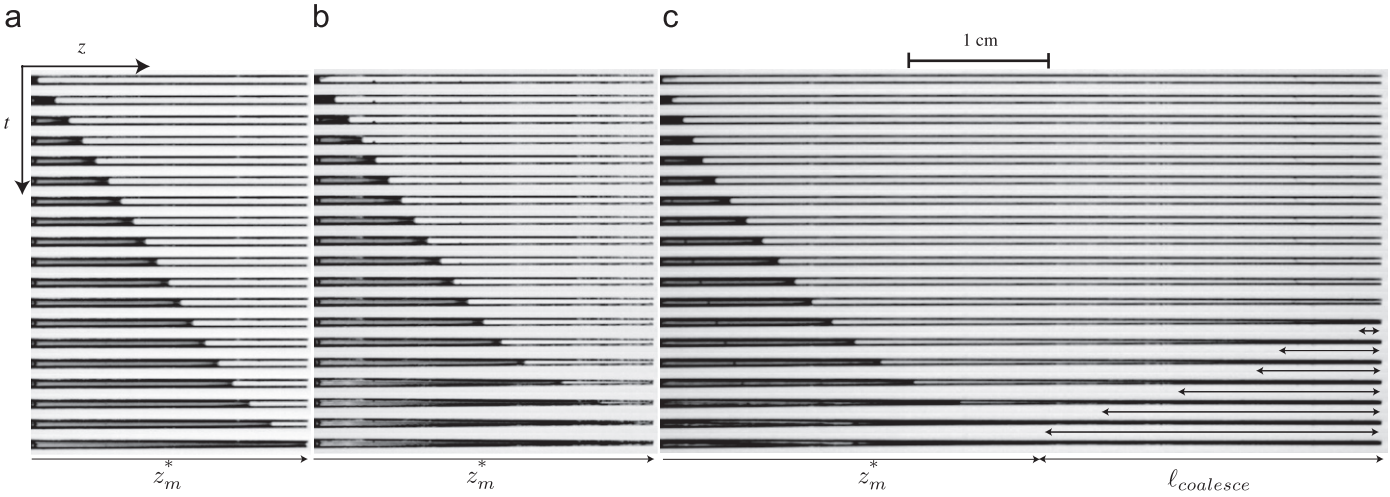


**Fig. 6.** Image sequences from the experiments of elastocapillary imbibition. Consecutive images (side views) are separated by a time interval $\Delta t$ for (a) $L=1.4$ (regime I), $\Delta t=3.3$ s, (b) $L=1.7$ (regime II), $\Delta t=2.8$ s and (c) $L=3.8$ (regime III), $\Delta t=4$ s, for silicon oil of viscosity $\mu=0.096$ Pa s. The arrows in (c) indicate the coalescence length $\ell_{coalesce}$.

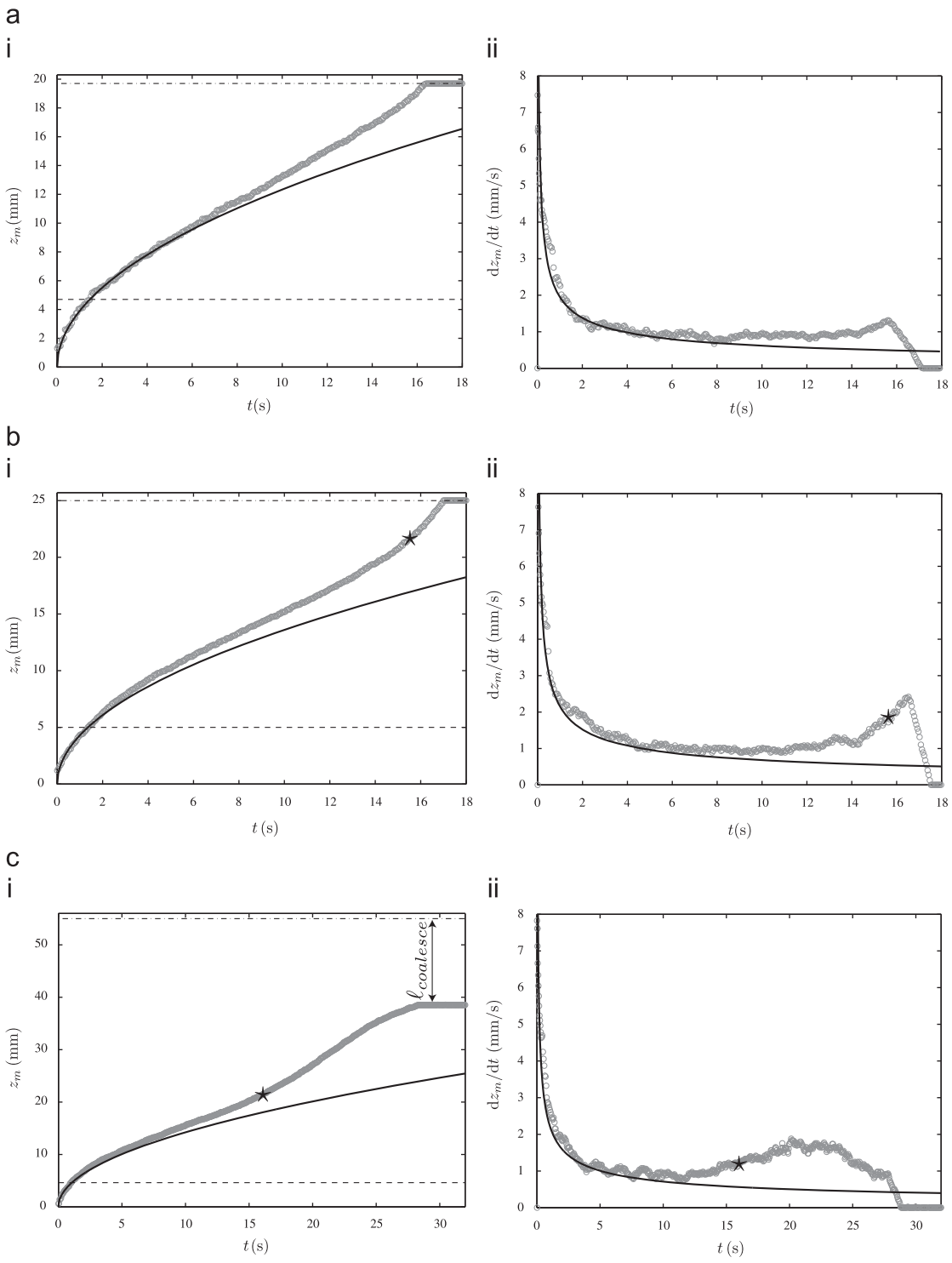


**Fig. 7.** Experimental observations of the evolution of the (i) position $z_m$ and (ii) speed $dz_m/dt$ of the meniscus with time for three values of $L=\ell/\ell_{ec}$ and silicone oil of viscosity $\mu=0.048$ Pa s. The solid lines correspond to the classical prediction $z_m=\alpha(at)^{1/2}$ and $dz_m/dt=(\alpha/2)(at)^{-1/2}$ with $a=2\gamma\cos\theta_e h_0/3\mu$ and a correction prefactor $\alpha=0.58$. The dashed lines correspond to the end of the clamped part of the sheets $z=\ell_0$, and the dash-dotted lines correspond to the end of the sheets $z=\ell+\ell_0$. In regimes II and III, the symbol $\star$ indicates the time at which the free ends of the sheets touch. (a) $L$=1.1 (regime I); (b) $L$=1.47 (regime II); (c) $L$=4.04 (regime III).

sheets becomes sufficiently large that toward the end of imbibition the free ends touch (Fig. 6b). The meniscus accelerates significantly and promptly stops at the closed end of the sheets (Fig. 7b).

In regime III ($2.5 \lesssim L \lesssim 4$), the sheets coalesce over a large distance during imbibition. As the ends touch, the liquid accelerates while the sheets start coalescing from the free end (Fig. 6c). The distance over which the sheets coalesce increases with time until the meniscus reaches the point of contact between the sheets and stops (Fig. 7c). In this regime, the meniscus gently slows down before stopping.

No clear dependence of the time at which imbibition stops $t^*$ with the sheet length is observed; nevertheless, the general trend indicates that $t^*$ increases with increasing $L$ for $L<4$, or with

Please cite this article as: J.M. Aristoff, et al., Elastocapillary imbibition, Int. J. Non-Linear Mech. (2010), doi:10.1016/j.ijnonlinmec.2010.09.001

increasing viscosity (data not shown). We note that although the final shape of the sheets does not correspond to an equilibrium configuration, it remains so indefinitely, an important feature should such a mechanism be used for applications is water storage. The three regimes observed in the experiments are in qualitative agreement with the numerical simulations. Further comparison is provided in the following section.

### 4.3. Data collapse

We measured the maximum penetration distance $z_m^* = Z_m^* \ell_{ec}$ at which the flow stops for several values of $L$ (Fig. 8). In regimes I and II, the meniscus reaches the end of the sheets ($Z_m^* = L$). Deviation from this behavior occurs for $L = 2.8$ when the sheets start coalescing over a significant distance. In regime III, the penetration distance attains a constant value $Z_m^* \simeq 2.5$. The evolution of $Z_m^*$ is in good agreement with the numerical simulations. However, the model slightly overestimates the critical value attained in regime III ($Z_m^* = 2.67$) as well as the sheet lengths at which the dynamics transition between adjacent regimes (see Fig. 4). The finite width and thickness of the sheets as well as the finite length $\ell_0$ necessary to clamp the sheets may account for this discrepancy. Nevertheless, we obtain a good agreement between experiment and numerical simulation.

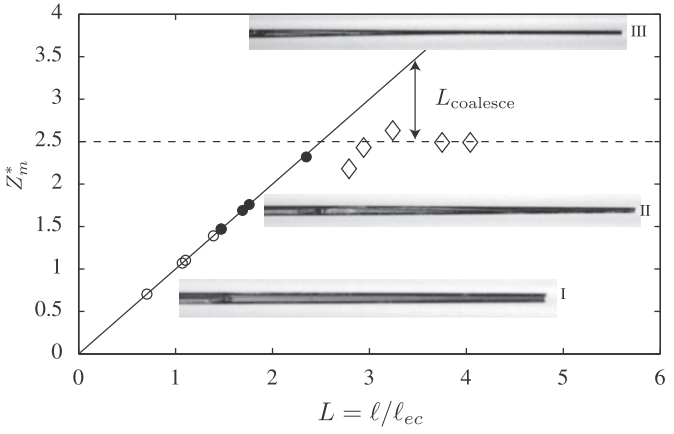


**Fig. 8.** Maximum penetration distance $Z_m^*$ as a function of the sheet length $L = \ell/\ell_{ec}$ in regimes I (◦), II (•) and III (◇). The solid line corresponds to $Z_m^* = L$. The dashed line corresponds to $Z_m^* = 2.5$, which is the mean distance at which imbibition stops in regime III, and is a value that appears roughly independent of $L$. The pictures depict the final observed shapes for $L = 1.4$ (regime I), $L = 1.7$ (regime II) and $L = 3.8$ (regime III).

We may now renormalize the data presented in Fig. 7 using $\ell_{ec}$ and $t_c$ as defined by (1) and (4), respectively. The resulting dimensionless presentation of the data is shown in Fig. 9. The data collapse onto a single curve at early times, when the meniscus follows the diffusive law $Z_m = \alpha\sqrt{2}T^{1/2}$. When $T$ and $Z_m$ become order one quantities, the imbibing front accelerates, in good agreement with the numerical prediction (Fig. 3) and scaling arguments presented in the previous sections.

## 5. Discussion

We have presented the results of a combined theoretical and experimental investigation of elastocapillary imbibition. In particular, we have examined the fluid flow between flexible sheets in the direction of the free ends, and have determined a criterion for capillary-driven coalescence. By treating the fluid flow as incompressible, viscous, and one-dimensional, and the solid deformation as linear and quasi-static, we have derived a coupled pair of evolution equations for the sheet profile and penetration distance. This non-linear free-boundary problem is solved numerically using finite-difference methods. In dimensionless form, the solution involves only a single parameter, the dimensionless sheet length $L = \ell/\ell_{ec}$. At early times, the boundary deflection is negligible, and we observe capillary-driven (classical) imbibition: the penetration distance increases with the square root of time, and the penetration speed decreases with the square root of time. At later times, the inward deflection of the sheets gives rise to an acceleration of the flow, followed by a closure of the gap at the meniscus. Consequently, the flow speed goes to zero in finite time, while the pressure at the meniscus goes to infinity. The final shape of the sheet therefore does not correspond to an equilibrium configuration. Further work could be done to analyze this singular structure.

Our study complements a recent report by van Honschoten et al. [15], who investigated imbibition into a nanochannel with an elastic capping layer. Since the capping layer was pinned along both sides of a channel, the deflection varied across the width of the channel and was maximum along its centerline. Consequently, contact between the capping layer and the channel bottom over the entire width of the channel could not occur, and the flow does not become blocked. However, the authors observe that as the deflection of the centerline increases, the penetration speed increases, a trend that is in agreement with our numerical results, albeit for a different geometry.

By considering the dynamics of elastocapillary imbibition, we have provided a framework in which to study more complicated problems regarding the coupling between capillary-driven flow and elastic boundaries, a number of which are currently under investigation. For

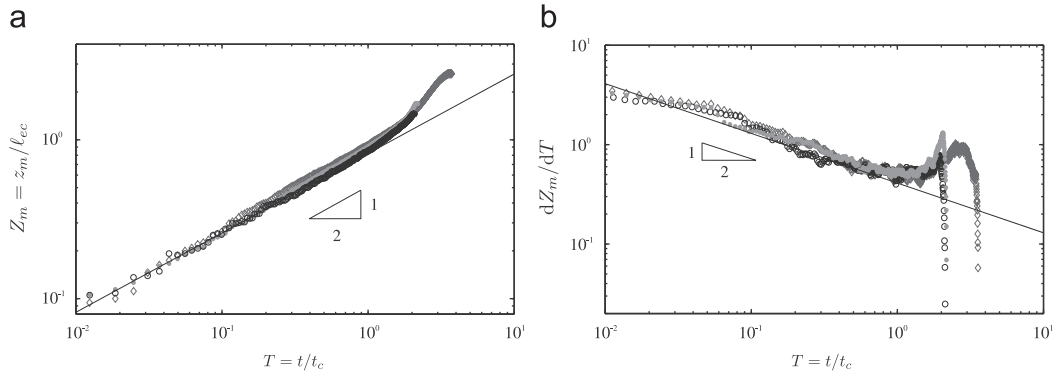


**Fig. 9.** Data collapse. (a) Renormalized position $Z_m = z_m/\ell_{ec}$ and (b) speed $dZ_m/dT$ of the meniscus as a function of time $T = t/t_c$ for $L = 1.1$ (regime I, black ◦), $L = 1.47$ (regime II, light gray •) and $L = 4.04$ (regime III, dark gray ◇). Solid lines correspond to the classical prediction $Z_m = \alpha\sqrt{2}T^{1/2}$ and $dZ_m/dT = (\alpha\sqrt{2}/2)T^{-1/2}$ with the correction factor $\alpha = 0.58$.

Please cite this article as: J.M. Aristoff, et al., Elastocapillary imbibition, Int. J. Non-Linear Mech. (2010), doi:10.1016/j.ijnonlinmec.2010.09.001

example, Bico et al. [11] and Kim and Mahadevan [12] considered the equilibrium shape following the elastocapillary rise of a liquid between flexible sheets. Recently, we have characterized the dynamics of elastocapillary rise by introducing gravity into our theoretical model and by solving numerically the resulting equations [23]. Other problems of interest include elastocapillary imbibition between surfaces with varying stiffness as well as between surfaces with non-zero curvature.

In what ways might elastocapillary mechanics (statics and dynamics) arise in nature? The manipulation and storage of water is paramount to the survival of plants and animals, which must periodically replenish their internal water content. We speculate that there exist biological structures that react to becoming wet by deforming in such a way as to reduce evaporation. For example, when a liquid drop is placed onto an elastic sheet, the sheet can spontaneously wrap itself around the drop [24]. Likewise, imbibition between flexible boundaries can lead to their coalescence and to the trapping of a liquid volume. For the case when the boundaries are initially parallel, we have determined the time scale and length scale necessary for coalescence. We have shown that above a critical sheet length, further increases in length do not increase the captured volume. Thus, our findings provide possible bounds on the size of a biological structure that exploits such an elastocapillary mechanism. In a broader sense, the transient wetting of flexible structures is relevant to hygromorphs, which are objects that deform in response to changes in environmental humidity. For example, the wilting of flowers, the wrinkling of skin, and the movement of wheat awns [25] are all induced by temporal fluctuations in environmental humidity. A fundamental understanding of these processes will continue to inform the design of biomimetic devices that can respond to external stimuli or that can manipulate liquids, an example of which is the elastocapillary pipette [26].

## Acknowledgments

J.M.A. gratefully acknowledges financial support from the National Science Foundation through the Mathematical Sciences Postdoctoral Research Fellowship. We thank I. Griffiths, and P. Warren and A. Lips at Unilever Research for helpful conversations. We are grateful for financial support from Unilever Research.

## References

[1] J.B. Grotberg, O.E. Jensen, Annu. Rev. Fluid Mech. 36 (2004) 121.
[2] A.L. Hazel, M. Heil, Proc. R. Soc. A 461 (2005) 1847.
[3] M. Heil, A.L. Hazel, J.A. Smith, Respir. Physiol. Neurobiol. 163 (2008) 214.
[4] T. Eisner, D.J. Aneshansley, Proc. Natl. Acad. Sci. 97 (2000) 6568.
[5] A.K. Geim, S.V. Dubonos, I.V. Grigorieva, K.S. Novoselov, Nat. Mater. 2 (2003) 461.
[6] C.H. Mastrangelo, C.H. Hsu, J. Microelectromech. Syst. 2 (1993) 33.
[7] T. Tanaka, M. Morigami, N. Atoda, Jpn. J. Appl. Phys. 32 (1993) 6059.
[8] N. Chakrapani, B. Wei, A. Carrillo, P.M. Ajayan, R.S. Kane, Proc. Natl. Acad. Sci. USA 101 (2004) 4009.
[9] O. Raccurt, F. Tardif, F.A. d'Avitaya, T. Vareine, J. Micromech. Microeng. 14 (2004) 1083.
[10] J.W.M. Bush, D.L. Hu, M. Prakash, Adv. Insect Physiol. 34 (2008) 118.
[11] J. Bico, B. Roman, L. Moulin, A. Boudaoud, Nature 432 (2004) 690.
[12] H.-Y. Kim, L. Mahadevan, J. Fluid Mech. 548 (2006) 141.
[13] H.-M. Kwon, H.-Y. Kim, J. Puëll, L. Mahadevan, J. Appl. Phys. 103 (2008) 093519.
[14] J.I. Siddique, D.M. Anderson, A. Bondarev, Phys. Fluids 21 (2009) 013106.
[15] J.W. van Honschoten, M. Escalante, N.R. Tas, H. Jansen, M. Elwenspoek, J. Appl. Phys. 101 (2007) 094310.
[16] M. Reyssat, L. Courbin, E. Reyssat, H.A. Stone, J. Fluid Mech. 615 (2008) 335.
[17] M.P. de Boer, T.A. Michalske, J. Appl. Phys. 86 (1999) 817.
[18] P.G. de Gennes, F. Brochard-Wyart, D. Quere, Capillarity and Wetting Phenomena: Drops, Bubbles, Pearls, Waves, Springer, 2003.
[19] G.K. Batchelor, An Introduction to Fluid Dynamics, Cambridge University Press, Cambridge, UK, 2000.
[20] L.D. Landau, E.M. Lifshitz, Theory of Elasticity, Pergamon Press, Oxford, UK, 1986.
[21] A.E. Hosoi, L. Mahadevan, Phys. Rev. Lett. 93 (2004) 137802.
[22] E. Guyon, J.P. Hulin, L. Petit, C.D. Mitescu, Physical Hydrodynamics, Oxford University Press, 2001.
[23] C. Duprat, J.M. Aristoff, H.A. Stone, arXiv:1008.3702v1 (2010).
[24] C. Py, P. Reverdy, L. Doppler, J. Bico, B. Roman, C.N. Baroud, Phys. Rev. Lett. 98 (2007) 156103.
[25] R. Elbaum, L. Zaltzman, I. Burgert, P. Fratzl, Science 316 (2007) 884.
[26] S. Jung, P.M. Reis, J. James, C. Clanet, J.W.M. Bush, Phys. Fluids 21 (2009).

Please cite this article as: J.M. Aristoff, et al., Elastocapillary imbibition, Int. J. Non-Linear Mech. (2010), doi:10.1016/j.ijnonlinmec.2010.09.001